Electrohydrodynamics within the electrical double layer in the presence of finite temperature gradients

Tanmay Ghonge,[1,*] Jeevanjyoti Chakraborty,[2,*] Ranabir Dey,[1,*] and Suman Chakraborty[1,2,†]
[1]*Mechanical Engineering Department, Indian Institute of Technology Kharagpur, Kharagpur-721302, India*
[2]*Advanced Technology Development Centre, Indian Institute of Technology Kharagpur, Kharagpur-721302, India*
(Received 7 December 2012; revised manuscript received 25 September 2013; published 26 November 2013)

A wide spectrum of electrokinetic studies is modeled as isothermal ones to expedite analysis even when such conditions may be extremely difficult to realize in practice. Going beyond the isothermal paradigm, we address here the case of flow induced electrohydrodynamics, commonly streaming potential flows, in a situation where finite temperature gradients do exist. By way of analyzing a model problem of flow through a narrow parallel-plate channel, we show that the temperature gradients applied at the channel walls may have a significant effect on the streaming potential, and, consequently, on the flow itself. Our model takes into consideration all the pertinent phenomenological aspects stemming from the imposed thermal gradients, such as the Soret effect, the thermoelectric effect, and the electrothermal effect, by a full-fledged coupling among the electric potential, the ionic species distribution, the fluid velocity and the local fluid temperature fields, without resorting to *ad hoc* simplifications. We expect this expository study to contribute significantly towards more sophisticated future endeavors in actual development of micro- and nano-devices for applications simultaneously involving thermal management and electrokinetic effects.

DOI: 10.1103/PhysRevE.88.053020 PACS number(s): 47.61.−k

I. INTRODUCTION

Streaming potential is one of the four primary electrokinetic phenomena, the other three being electro-osmosis, electrophoresis, and sedimentation potential. The genesis of these phenomena is contingent on the development of an electrical double layer (EDL) which refers to the space charge distribution in a dielectric medium together with the electrified surface in whose immediate vicinity such distribution is established through a balance between Coulombic and entropic interactions [1]. The particular phenomenon of streaming potential is, however, set apart by the fact that its manifestation does not depend on the application of an external field (unlike electro-osmosis and electrophoresis) nor does it involve the transport of particles bearing such electrified surfaces (unlike electrophoresis and sedimentation potential). As long as flow (actuated through simple mechanical actuation) of fluid, bearing the space charge distribution, takes place past the electrified surface, a streaming current will be always generated, and given a scope of charge accumulation through the specific geometry, a streaming potential will also develop together with such current.

Indeed, it is because of this apparent simplicity that ever since the discovery of this phenomenon more than 150 years ago by Quincke [2], streaming potential has been found to be a key element in the explanation of various phenomena in areas as diverse as physiological [3–5] to geophysical [6]. It has also been used in a host of applications in the colloidal science realm; for instance, zeta potential measurement and electrokinetic characterization of surfaces [7–11]. Most recently, it has provided a new direction in the search for innovative energy conversion techniques [12–39]. Nevertheless, despite the long and what would otherwise seem an "established" history [40–45], ongoing research efforts continue to further our fundamental understanding of streaming potential, as well to extend the possibilities of its use together with a slew of additional surface and flow characteristics [46–65].

Interestingly, such research and modeling efforts have been carried out, almost without exception, with the unquestioned assumption that the systems under consideration are isothermal. This is despite the ubiquity of nonisothermal natural settings, and also in spite of the fact that even in laboratory settings, perfect isothermal conditions are difficult to realize in practice. Such an approach is paradigmatic of most of the electrokinetic modeling efforts inasmuch as it pertains to the microfluidic and nanofluidic contexts. However, it must be noted here that there do exist numerous works which are indeed concerned with temperature variations within the electrokinetic framework. However, these involve simplistic one-way couplings [66–71], or, at best, couplings between momentum and energy through temperature-dependent thermophysical properties [72–74]. Importantly, they do not consider the fundamental dependence of the ionic fluxes on the temperature variation, and the ramifications thereof. This situation is rather surprising, particularly when considered in the context of the rich theory that already exists to model coupled momentum, mass, and thermal transport based on general nonequilibrium thermodynamic principles [75,76]. Such general theories have routinely been adapted to represent various transport phenomena involved in membrane technology [77]. Investigations involving nonisothermal transport are also quite common in electrochemical systems under the purview of thermoelectrochemistry [78], particularly at high temperatures [79]. On another front, certain fundamental modeling frameworks have also been developed under the purview of colloidal science [80,81]. Despite the obvious commonalities that exist between these areas and micro- and nanofluidics, the modeling of nonisothermal electrokinetic transport through micro- and nanochannels, in general, and streaming potential mediated nonisothermal transport in particular has remained largely unaddressed [82].

*T.G., J.C., and R.D. contributed equally to the work.
†Corresponding author: suman@mech.iitkgp.ernet.in

It is only in the last few years that successful attempts have been made to capture the fundamental influences of temperature gradient on the flux of the ionic species itself [83–93], following the strategy by Guthrie *et al*. [94]. Notable precursors to these works were the ones by Ruckenstein [95] and Morozov [96]. These works have also motivated the application of thermal gradients for controlled manipulation of particle motion in microfluidic channels [97]. While the modeling efforts in these works are directed towards the transport of colloidal particles and are, hence, reminiscent of the aforementioned earlier works [80,81], important differences do exist in the approach itself [87]. In contrast to the previous works which involve a dependence on the enthalpy in the velocity expression, these recent efforts express the velocity in terms of the temperature gradient in an explicit and straightforward way. This is done by taking into account the contribution of the Soret effect, which refers to the motion of a particle when placed in a temperature gradient [98,99], directly in the flux. When the particle itself is charged (as in the case of an ionic species) such transport may work together with conventionally recognized responses to concentration and electrical potential gradients to generate novel flow characteristics.

The influences of the rich interplay among these various factors under conditions of dynamic equilibrium are particularly intriguing in the case of streaming potential mediated flow. This is because it holds the possibility of unveiling new and nonintuitive flow characteristics in the otherwise routine, primarily pressure-gradient actuated flow through the simple application of a temperature gradient. This motivates the primary objective of the current study: to investigate the influence of an externally applied temperature gradient on a pressure-gradient-driven flow of an electrolyte solution which also results in the generation of a streaming potential. Notwithstanding the apparent simplicity of such an objective, the scope of this investigation is far reaching owing to its rigorous and exhaustive treatment of the involved physical phenomena inherent in the system.

In this study, we delineate the specific extent to which the Soret effect, and the consequential Seebeck effect (having its genesis in different values of the ionic heats of transport of the cations and the anions)—which, in turn, leads to the thermoelectric field—influence the streaming potential mediated flow. Furthermore, we unequivocally show that the degree of Soret effect induced alteration of the resulting flow rate is intimately dependent on the electrothermal effect, ubiquitous in such nonisothermal systems. In essence, the primary finding of this work is that within the general nonisothermal electrokinetic framework, it is possible to control (either augment or negate) the volumetric suppression of the primary pressure-driven flow, due to the streaming potential field, by judicious tuning of the Seebeck effect. Interestingly, such control over the nature of the streaming potential mediated flow is achieved simply on the basis of the electrolyte nature, without changing the applied temperature gradient.

The remaining part of this article is organized as follows. In Sec. II, we describe the model problem for analyzing the influence of temperature gradient on streaming potential modulated flows. We also outline the general equations governing the electrical potential, the ionic species distribution (incorporating thermoelectric effects), the fluid-flow equations, and the energy equation that need to be solved in a coupled way, considering the thermophysical property variations with temperature, for a resolution of the intrinsic interdependence among the various fields. Additionally, in this section, we derive the electric field associated with the streaming potential incorporating the thermoelectric effect. For brevity, we also present in Sec. II the dimensionless versions of all the governing equations, and the adopted nondimensional scheme, along with the corresponding dimensional forms. In Sec. III, we discuss the pertinent boundary conditions. In Sec. IV, we report and discuss the major findings of our investigation. Finally, in Sec. V, we draw important conclusions based on these findings.

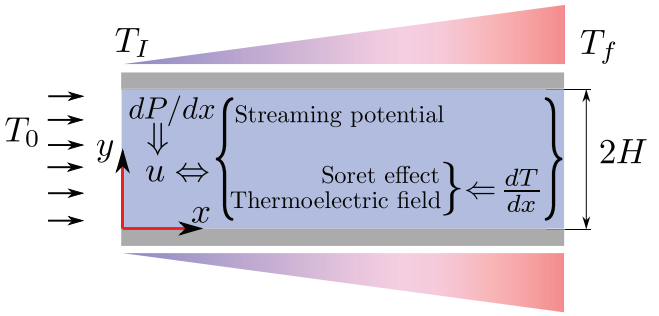

FIG. 1. (Color online) Schematic of the problem geometry.

II. MATHEMATICAL FORMULATION

Steady, incompressible, and laminar pressure-driven transport of a Newtonian fluid, containing symmetric electrolytes ($z_+ = -z_- = z$), through a long, parallel-plate channel of height $2H$, length L, and width W ($W \gg 2H$) is considered here (See Fig. 1). The flow is actuated by a constant axial pressure gradient, $P_x = -dP/dx$. The fluid enters the channel at temperature T_0 with a uniform velocity. The tip of the plate where the fluid enters is maintained at temperature T_1. There is an imposed linear temperature gradient on both the plates. The temperature of the tip of the channel where the fluid leaves is T_f.

A. Potential distribution

The electrostatic potential, ψ, in the diffuse layer of EDL is governed by the Poisson equation: $\nabla \cdot (\epsilon \nabla \psi) = -\rho_e$, where ϵ is the temperature-dependent permittivity of the medium, and $\rho_e = ez(n_+ - n_-)$ is the free charge density, with e being the electronic charge magnitude, and n_+ and n_- the number density of the positive and the negative ions respectively. Now, we use the nondimensional variables: $\tilde{\psi} = ez\psi/(4k_BT_0)$, $\tilde{n}_\pm = n_\pm/n_0$, $\tilde{x} = x/L$, $\tilde{y} = y/H$, and $\tilde{\epsilon} = \epsilon/\epsilon_0$, where k_B is the Boltzmann constant, n_0 is the bulk value of the number density of the electrolyte, and ϵ_0 is the permittivity at $T = T_0 = 298$ K, to reduce the Poisson equation to its corresponding dimensionless version:

$$\alpha^2 \frac{\partial}{\partial \tilde{x}}\left(\tilde{\epsilon}\frac{\partial \tilde{\psi}}{\partial \tilde{x}}\right) + \frac{\partial}{\partial \tilde{y}}\left(\tilde{\epsilon}\frac{\partial \tilde{\psi}}{\partial \tilde{y}}\right) = -\frac{1}{8}K^2(\tilde{n}_+ - \tilde{n}_-), \qquad (1)$$

where $\alpha = H/L$ is the aspect ratio of the channel, and $K = H/\lambda_0$ is the ratio of the half height of the channel to the Debye screening length $\lambda_0 = \sqrt{\epsilon_0 k_B T_0/(2n_0 e^2 z^2)}$ (based on the permittivity value at T_0). It is to be noted here that the factor 4, considered during nondimensionalizing the electrostatic potential, is in accordance with Ref. [48]. This helps in casting the pertinent equations into forms analogous to that present in Ref. [48], which consequently facilitates the validation of the present solution procedure (discussed later in Sec. IV). The use of the factor 4 just simplifies the resulting mathematical expressions, as can be perceived in the existing literature, and has no physical significance.

B. Species transport

The general species transport equation routinely invoked in continuum descriptions of electrokinetic phenomena is $\frac{\partial n_\pm}{\partial t} = -\nabla \cdot \mathbf{j}_\pm$, where $\mathbf{j}_\pm$ is the flux of the cation and the anion. Here, an important assumption is that there is no source term due to generation or consumption of any ionic species by any bulk reaction within the electrolyte. In conventional isothermal treatments, this flux arises as a combination of diffusion, electromigration, and advection [100]. However, in the present case, there is an additional contribution to the flux from the temperature gradient. Physically, this comes about due to the propensity of a species to move in response to gradients in the temperature field, and is classically referred to as the Soret effect. This has rich implications in the resulting physical scenario, for this motion of the ionic species due to the temperature field may itself result in the generation of an electric potential especially when the thermal diffusivities of the ionic species, with different polarities of charge on them, are different. The generation of this thermoelectric potential is analogous to the Seebeck effect. The total electric potential which influences the ionic flux is, thus, a combination of the intrinsic electrokinetic screening potential and the thermoelectric potential together with the streaming potential which is induced parallel to the flow direction as a result of the streaming motion of the ions associated with the pressure-driven fluid flow. Hence, the resultant species transport is an intimately coupled manifestation of this combined electric potential, the temperature gradient, the gradients in the concentration (which is itself coupled to the potential through the Poisson equation), and the advection associated with the fluid motion (which, as we show later, is, again, influenced by the electric potential and concentration gradients). To address this highly coupled phenomenon, we first note that the flux of the ionic species may be expressed as [84]

$$\mathbf{j}_\pm = n_\pm \mathbf{u} - D_\pm \left[\nabla n_\pm + \frac{n_\pm Q_\pm}{k_B T^2} \nabla T \pm \frac{n_\pm e z}{k_B T} (\nabla \psi - \mathbf{E}_s) \right], \tag{2}$$

where $\mathbf{u}$ is the mean fluid velocity, $\mathbf{E}_s$ is the electric field associated with the streaming potential (it must be noted here that the generated thermoelectric potential is incorporated within $\mathbf{E}_s$), $D_\pm$ denote the temperature-dependent diffusivities of the positive and the negative ions, and $Q_\pm$ denote the ionic heat of transport of the positive and the negative ions. The second term between brackets on the right-hand side in Eq. (2) represents the contribution of the Soret effect. Then, at steady state, the transport equations for ions reduce simply to $\nabla \cdot \mathbf{j}_\pm = 0$. Augmenting the nondimensionalization scheme mentioned previously with the definitions, $\tilde{D}_\pm = D_\pm/D_\pm^0$ (where $D_\pm^0$ are the ionic diffusivities at T_0), $\tilde{u} = u/u_{\mathrm{ref}}$, and $\tilde{T} = T/T_0$, we have the following forms of the dimensionless species transport equations:

$$\begin{aligned} 0 = &-\left[\alpha^2 \frac{\partial}{\partial \tilde{x}}\left(\tilde{D}_+ \frac{\partial \tilde{n}_+}{\partial \tilde{x}}\right) + \frac{\partial}{\partial \tilde{y}}\left(\tilde{D}_+ \frac{\partial \tilde{n}_+}{\partial \tilde{y}}\right)\right] \\ &+ \frac{\partial}{\partial \tilde{y}}\left[\left(-\frac{4\tilde{D}_+}{\tilde{T}}\frac{\partial \tilde{\psi}}{\partial \tilde{y}} - \mathcal{Q}\frac{\partial \tilde{T}}{\partial \tilde{y}}\frac{\tilde{D}_+}{\tilde{T}^2}\right)\tilde{n}_+\right] \\ &+ \alpha^2 \frac{\partial}{\partial \tilde{x}}\left[\left(-\frac{4\tilde{D}_+}{\tilde{T}}\frac{\partial \tilde{\psi}}{\partial \tilde{x}} + \frac{\tilde{D}_+}{\tilde{T}}\tilde{E}_s - \mathcal{Q}\frac{\partial \tilde{T}}{\partial \tilde{x}}\frac{\tilde{D}_+}{\tilde{T}^2}\right)\tilde{n}_+\right] \\ &+ \alpha \mathrm{Pe}\frac{\partial(\tilde{n}_+\tilde{u})}{\partial \tilde{x}}, \end{aligned} \tag{3}$$

$$\begin{aligned} 0 = &-\left[\alpha^2 \frac{\partial}{\partial \tilde{x}}\left(\tilde{D}_- \frac{\partial \tilde{n}_-}{\partial \tilde{x}}\right) + \frac{\partial}{\partial \tilde{y}}\left(\tilde{D}_- \frac{\partial \tilde{n}_-}{\partial \tilde{y}}\right)\right] \\ &+ \frac{\partial}{\partial \tilde{y}}\left[\left(\frac{4\tilde{D}_-}{\tilde{T}}\frac{\partial \tilde{\psi}}{\partial \tilde{y}} - \gamma\mathcal{Q}\frac{\partial \tilde{T}}{\partial \tilde{y}}\frac{\tilde{D}_-}{\tilde{T}^2}\right)\tilde{n}_-\right] \\ &+ \alpha^2 \frac{\partial}{\partial \tilde{x}}\left[\left(\frac{4\tilde{D}_-}{\tilde{T}}\frac{\partial \tilde{\psi}}{\partial \tilde{x}} - \frac{\tilde{D}_-}{\tilde{T}}\tilde{E}_s - \gamma\mathcal{Q}\frac{\partial \tilde{T}}{\partial \tilde{x}}\frac{\tilde{D}_-}{\tilde{T}^2}\right)\tilde{n}_-\right] \\ &+ \alpha D_r \mathrm{Pe}\frac{\partial(\tilde{n}_-\tilde{u})}{\partial \tilde{x}}, \end{aligned} \tag{4}$$

where $\mathrm{Pe} = u_{\mathrm{ref}} H/D_+^0$ is the Péclet number based on the cationic diffusivity at T_0 (u_{ref} is defined later), $D_r = D_+^0/D_-^0$ is the ratio of the diffusivity values at T_0, $\mathcal{Q} = Q_+/k_B T_0$ and $\gamma = Q_-/Q_+$ is the ratio of the ionic heats of transport.

C. Streaming potential field

The downstream migration of ions due to the flow primarily actuated by the imposed pressure gradient gives rise to a current known as the streaming current (I_s). However, in the stationary state, this convective transport of ions sets up its own electric potential known as the streaming potential. The electric field (E_s) associated with this streaming potential generates a current, known as the conduction current (I_c). Much like the electro-osmotic flow situation, this conduction current, in turn, leads to a fluid flow opposite to the pressure-driven flow which is responsible for inducing the same in the first place. In the absence of an externally imposed electric field, the conduction current and the streaming current must balance each other so that the net ionic current in the system along the axial direction is zero; thus

$$I_{\mathrm{ionic}} = I_s + I_c = 0. \tag{5}$$

It is important to realize here that the real physical situation is far more involved than the aforementioned simplistic description. The intricacy stems from the interplay among the electric potential (with contributions from the electrokinetic screening potential, the thermoelectric potential, and the streaming potential), the concentration profiles, the velocity and the temperature fields (the latter being also responsible for providing an additional coupling among the pertinent physical fields through thermophysical property variations with temperature). However, in spite of the inherent complexity, the only requirement that needs to be necessarily satisfied is that

the total ionic current along the axial direction, at any cross section of the channel, vanishes. In order to capture this general requirement, we express the local ionic current in terms of the axial direction components of the cationic and the anionic fluxes:

$$i = ez(j_{+x} - j_{-x}), \tag{6}$$

so that the total ionic current across a cross section of the channel is given by

$$I_{\text{ionic}} = ez \int_0^{2H} (j_{+x} - j_{-x}) dy. \tag{7}$$

Thereafter, imposing the condition of the vanishing total ionic current, we obtain an expression for the electric field, E_s, associated with the streaming potential in the following dimensionless form:

$$\tilde{E} = \frac{ezL}{k_B T_0} E_s = \frac{-\frac{1}{\alpha} D_r \text{Pe} I_1 + I_2 + I_3 + \mathcal{Q} I4}{I_5}, \tag{8}$$

where the streaming potential field has been nondimensionalized by $k_B T_0/ezL$, and the expressions of the various integrals are

$$I_1 = \int_0^2 (\tilde{n}_+ - \tilde{n}_-)\tilde{u} d\tilde{y}, \tag{9}$$

$$I_2 = \int_0^2 \left(D_r \tilde{D}_+ \frac{\partial \tilde{n}_+}{\partial \tilde{x}} - \tilde{D}_- \frac{\partial \tilde{n}_-}{\partial \tilde{x}} \right) d\tilde{y}, \tag{10}$$

$$I_3 = \int_0^2 4 \left(\frac{D_r \tilde{D}_+ \tilde{n}_+ + \tilde{D}_- \tilde{n}_-}{\tilde{T}} \right) \frac{\partial \tilde{\psi}}{\partial \tilde{x}} d\tilde{y}, \tag{11}$$

$$I_4 = \int_0^2 \left(\frac{D_r \tilde{D}_+ \tilde{n}_+ - \gamma \tilde{D}_- \tilde{n}_-}{\tilde{T}^2} \right) \frac{\partial \tilde{T}}{\partial \tilde{x}} d\tilde{y}. \tag{12}$$

The important thing to note here is that this is not an explicit expression because the velocity field in the integral I_1 depends on this streaming potential field itself. To determine this dependence, we next move on to a description of the velocity fields from the Navier-Stokes equations representing the momentum transport of the fluid.

D. Velocity field

The axial advection contributing to the flux and, hence, to the streaming potential field is governed by the x-momentum equation which under the assumption of low Reynolds number flow reduces to

$$0 = \frac{-dP}{dx} + \frac{\partial}{\partial x}\left(\mu \frac{\partial u}{\partial x} \right) + \frac{\partial}{\partial y}\left(\mu \frac{\partial u}{\partial y} \right) + F_x, \tag{13}$$

where μ is the temperature-dependent dynamic viscosity, and F_x is the total body force, which is made up of three contributions: first, F_{O_x} due to the osmotic pressure; second, F_{E_x} due to the Maxwell stress along the axial direction; and third, F_{ETx} due to the electrothermal contribution (stemming from the electrical permittivity variations with temperature). Noting that the general expression of force due to osmotic pressure is $\mathbf{F}_O = -\nabla[(n_+ + n_-)k_B T]$, the x component of this force is

$$F_{O_x} = -k_B(n_+ + n_-)\frac{\partial T}{\partial x} - k_B T \frac{\partial (n_+ + n_-)}{\partial x}. \tag{14}$$

It is, therefore, this contribution from the osmotic pressure which takes into account the dependence of the velocity field on the temperature gradient as well as the concentration gradients that are established as a combined consequence of the electrokinetic and Soret effects. Next, the general expression for the contribution of the Maxwell's stress to the body force is $\mathbf{F}_E = \epsilon \nabla^2 \phi \nabla \phi$, where the total potential $\phi = \phi_0 + \psi$, and $\nabla \phi_0 = -\mathbf{E}_s$. Further, we note that $\nabla^2 \phi \approx \partial_y^2 \psi$ because ϕ_0 is constant along the transverse direction and both ϕ_0 and ψ are assumed to weakly vary along the x direction. Under these considerations, the axial component of this force becomes

$$F_{E_x} = \left[\frac{\partial}{\partial x}\left\{ \epsilon \left(-E_s + \frac{\partial \psi}{\partial x} \right) \right\} + \frac{\partial \epsilon}{\partial y}\frac{\partial \psi}{\partial y} + \epsilon \frac{\partial^2 \psi}{\partial y^2} \right] \times \left(-E_s + \frac{\partial \psi}{\partial x} \right). \tag{15}$$

The general expression of the force due to the electrothermal contribution is $\mathbf{F}_{ET} = -\frac{1}{2}|\mathbf{E}|^2 \nabla \epsilon$ so that the axial component becomes

$$F_{ETx} = -\frac{1}{2}\left[\left(E_s - \frac{\partial \psi}{\partial x} \right)^2 + \left(\frac{\partial \psi}{\partial y} \right)^2 \right] \frac{\partial \epsilon}{\partial x}. \tag{16}$$

Using Eqs. (14)–(16) in Eq. (13), and the previously described nondimensionalization scheme together with the definition $\tilde{\mu} = \mu/\mu_0$ (where μ_0 is the dynamic viscosity at T_0), the dimensionless version of the x-momentum equation becomes

$$\begin{aligned} 0 = {} & 2 + \left[\alpha^2 \frac{\partial}{\partial \tilde{x}}\left(\tilde{\mu} \frac{\partial \tilde{u}}{\partial \tilde{x}} \right) + \frac{\partial}{\partial \tilde{y}}\left(\tilde{\mu} \frac{\partial \tilde{u}}{\partial \tilde{y}} \right) \right] - C \frac{\partial}{\partial \tilde{x}}(\tilde{n}\tilde{T}) \\ & + 2\frac{C}{K^2}\left[\alpha^2 \frac{\partial \tilde{\varepsilon}}{\partial \tilde{x}}\left(-\tilde{E}_S + 4\frac{\partial \tilde{\psi}}{\partial \tilde{x}} \right) + 4\frac{\partial \tilde{\varepsilon}}{\partial \tilde{y}}\frac{\partial \tilde{\psi}}{\partial \tilde{y}} + 4\tilde{\varepsilon}\frac{\partial^2 \tilde{\psi}}{\partial \tilde{y}^2} \right] \\ & \times \left(-\tilde{E}_S + 4\frac{\partial \tilde{\psi}}{\partial \tilde{x}} \right) \\ & - \frac{C}{K^2}\left[\alpha^2 \left(\tilde{E}_S - 4\frac{\partial \tilde{\psi}}{\partial \tilde{x}} \right)^2 + 16\left(\frac{\partial \tilde{\psi}}{\partial \tilde{y}} \right)^2 \right] \frac{\partial \tilde{\varepsilon}}{\partial \tilde{x}}, \end{aligned} \tag{17}$$

where $C = \frac{2n_0 k_B T_0}{-LdP/dx}$ represents the strength of the osmotic pressure relative to that of the hydrodynamic pressure, and u_{ref} can now be defined as $u_{\text{ref}} = \frac{P_x H^2}{2\cdots_0}$.

E. Temperature field

Taking into consideration the effects of axial conduction and viscous dissipation the thermal transport equation can be written as

$$\rho C_p u \frac{\partial T}{\partial x} = \frac{\partial}{\partial x}\left(k \frac{\partial T}{\partial x} \right) + \frac{\partial}{\partial y}\left(k \frac{\partial T}{\partial y} \right) + \mu \left(\frac{\partial u}{\partial y} \right)^2, \tag{18}$$

where ρ is the density, C_p is the specific heat capacity, and k is the temperature-dependent thermal conductivity of the electrolyte. Again using the nondimensionalization scheme mentioned previously with the added definition $\tilde{k} = k/k_0$ (where k_0 is the thermal conductivity at T_0), we obtain the

dimensionless version of Eq. (18) as

$$\alpha \mathrm{Pe}_T \tilde{u}\frac{\partial \tilde{T}}{\partial \tilde{x}} = \frac{\partial}{\partial \tilde{y}}\left(\tilde{k}\frac{\partial \tilde{T}}{\partial \tilde{y}}\right) + \alpha^2 \frac{\partial}{\partial \tilde{x}}\left(\tilde{k}\frac{\partial \tilde{T}}{\partial \tilde{x}}\right) + \mathrm{Br}_R \tilde{\mu}\left(\frac{\partial \tilde{u}}{\partial \tilde{y}}\right)^2, \tag{19}$$

where $\mathrm{Pe}_T = \frac{\rho C_p u_{\mathrm{ref}} H}{k_0}$, is the thermal Péclet number, and $\mathrm{Br}_R = \frac{\mu_0 u_{\mathrm{ref}}^2}{k_0 T_0}$ is the Brinkman number based on T_0. It must be noted here that the classical Joule heating term in the energy equation is outweighed by the viscous dissipation term for the physical problem under consideration. This can be easily concluded from a simple order of magnitude analysis of the two physical quantities. In accordance with the ongoing analysis, the viscous dissipation term scales as $\mu_0 u_{\mathrm{ref}}^2/H^2$ (where $u_{\mathrm{ref}} = \frac{P_x H^2}{2\mu_0}$), while the Joule heating term scales as $\frac{z^2e^2D}{k_B T_0} 2n_0 E_s^2$ [78]. Hence, the ratio of these two quantities comes out to be $\frac{\text{Viscous dissipation}}{\text{Joule heating}} \sim \frac{1}{4K^2}\frac{P_x^2 H^4}{\epsilon D \mu_0 E_s^2}$. Now, using $K = 10$ and $E_s = \frac{\tilde{E}_s k_B T_0}{ezL}$ with $\tilde{E}_s \sim 1$ to be a representative value of the nondimensional streaming potential field, along with the physically consistent values of the other involved parameters (mentioned in detail later), we find that the value of the ratio is >150. Therefore, the neglect of the Joule heating term in comparison to the viscous dissipation term, as done here, stems directly from the physical condition under consideration, and is in no way an *ad hoc* simplification which compromises the generality of the problem. However, it is important to note here that the ratio of viscous dissipation to Joule heating is dependent on the parameters H (which is fixed by the choice of K and λ_0) and n_0. The aforementioned order of magnitude analysis holds true for electrolyte concentrations ~10 mM, which is very much within the physically realizable range for electrokinetic experiments. However, for even higher concentrations of the electrolyte solution, the above ratio decreases and Joule heating may play an important role.

III. BOUNDARY CONDITIONS

A. Wall

A linear temperature gradient is applied along the channel wall [$T = T_1 + (T_f - T_1)x/L$]. The wall is considered to be an impenetrable boundary so that there is no flux of ions across it ($\hat{n} \cdot \mathbf{j}_\pm = 0$), with $\hat{n}$ depicting the unit vector normal to the surface. Further, no-slip boundary condition is assumed: $u = 0$ at the wall. In dimensionless form these boundary conditions at the wall ($\tilde{y} = 0$ and $0 \leqslant \tilde{x} \leqslant 1$) are expressed as

$$\begin{aligned} &\tilde{T} = \tilde{T}_1\{1 + \tilde{x}(T_{\mathrm{ratio}} - 1)\}, \\ &\frac{\partial \tilde{n}_\pm}{\partial \tilde{y}} \pm 4\left(\frac{n_\pm}{\tilde{T}}\frac{\partial \tilde{\psi}}{\partial \tilde{y}}\right) + \frac{Q_\pm}{k_B T_0}\left(\frac{\tilde{n}_\pm}{\tilde{T}^2}\frac{\partial \tilde{T}}{\partial \tilde{y}}\right) = 0, \\ &\tilde{u} = 0, \end{aligned} \tag{20}$$

where $T_{\mathrm{ratio}} = T_f/T_1$. It is important to note that the electrical potential boundary condition on the wall (zeta potential, ζ) involves a variation along the wall because of its temperature dependence. Such variation of the zeta potential with the temperature has been extensively studied in the geophysical context. Ishido and Mizutani [101] presented a comprehensive experimental and theoretical treatment of temperature-dependent zeta potential. They found that for quartz, in an aqueous solution of $10^{-3}N$ KNO_3 with a pH of 6.1, the zeta potential increases in magnitude by 3.3 mV/10 °C. Later, more sophisticated modeling efforts by Revil *et al.* [102] and Reppert and Morgan [103] that included extensive use of chemical equilibria conditions were validated against the primary results of Ishido and Mizutani. Considering this to be representative of the paradigmatic combination of SiO_2 surface in physical contact with a binary symmetric electrolyte widely used in microfluidic applications, we use the temperature-dependent variation of zeta potential as proposed by Ishido and Mizutani. Importantly, we do not unnecessarily incorporate the rather involved chemical equilibria-based modeling in our framework with the understanding that the ultimate denouement of such complicated developments is indeed the simple relation given by [101]

$$\frac{d\zeta}{dT} = \mathrm{sgn}(\zeta)g, \tag{21}$$

where $g = 3.3 \times 10^{-4}$ V K^{-1}. Using this, the dimensionless form of the boundary condition on the wall becomes

$$\tilde{\zeta} = \tilde{\zeta}_0 + \tilde{g}\,\mathrm{sgn}(\zeta)\tilde{T}_1(T_{\mathrm{ratio}} - 1)\tilde{x}, \tag{22}$$

where $\{\tilde{\zeta}, \tilde{\zeta}_0\} = ez/4k_BT\{\zeta, \zeta_0\}$, with ζ_0 the zeta potential at the left tip of the wall, $\tilde{g} = ezg/4k_B$, and $\tilde{T}_1 = T_1/T_0$.

B. Centerline

At the channel centerline, we assume far-stream condition ($\psi = 0$) together with the electroneutrality condition: $n_\pm = n_0$. Since the characteristic EDL penetration depths under consideration are smaller than the channel half height, the channel centerline does not "feel" the charging effect of the wall, so that the boundary conditions $\psi = 0$ and $\partial\psi/\partial y = 0$ are equivalent. Exploiting the symmetry of the channel about the centerline, we set the gradient of the velocity and the temperature gradient in the transverse direction to be zero: $\partial u/\partial y$ and $\partial T/\partial y = 0$. In dimensionless form, these boundary conditions at the centerline ($\tilde{y} = 1$ and $0 \leqslant \tilde{x} \leqslant 1$) are given by

$$\tilde{\psi} = 0, \quad \tilde{n}_\pm = 1, \quad \frac{\partial \tilde{u}}{\partial \tilde{y}} = 0, \quad \frac{\partial \tilde{T}}{\partial \tilde{y}} = 0. \tag{23}$$

C. Entrance

We assume the fluid to enter the channel at a temperature $T = T_0$ (uniform), with a uniform velocity (we take this to be $u = 0.1u_{\mathrm{ref}}$), and ionic concentration equal to the bulk concentration ($n_\pm = n_0$). In dimensionless form, the boundary conditions at the entrance ($0 \leqslant \tilde{y} \leqslant 1$ and $\tilde{x} = 0$) are given by

$$\tilde{n}_\pm = 1, \quad \tilde{u} = 0.1, \quad \tilde{T} = 1. \tag{24}$$

D. Exit

We consider the channel exit condition to be such that there are no axial gradients in the flow ($\frac{\partial \tilde{u}}{\partial \tilde{x}} = 0$), and that the ionic concentration at the exit is equal to the bulk concentration ($n_\pm = n_0$). The temperature profile at the exit is derived from

the energy conservation principle (i.e., the energy leaving the control volume is the sum of the energy entering the control volume and the energy generated through viscous dissipation). Thus, at the exit ($0 \leqslant \tilde{y} \leqslant 1$ and $\tilde{x} = 1$) we have the following dimensionless form of the boundary conditions:

$$\begin{aligned} &\tilde{\psi} = 0, \quad \tilde{n}_{\pm} = 1, \quad \frac{\partial \tilde{u}}{\partial \tilde{x}} = 0, \\ &\alpha \mathrm{Pe}_T \int_0^1 \tilde{u}(0,\tilde{y})\tilde{T}(0,\tilde{y})d\tilde{y} - \int_0^1 \tilde{k}\frac{\partial \tilde{T}}{\partial \tilde{y}}d\tilde{x} \\ &\quad + \mathrm{Br}_R \int_0^1 \int_0^1 \tilde{\mu}\left(\frac{\partial \tilde{u}}{\partial \tilde{y}}\right)^2 d\tilde{x}d\tilde{y} \\ &\quad = \alpha \mathrm{Pe}_T \int_0^1 \tilde{u}(1,\tilde{y})T(1,\tilde{y})d\tilde{y}. \end{aligned} \tag{25}$$

IV. RESULTS AND DISCUSSIONS

The primary objective of the present work is to investigate the influence of temperature gradients on streaming potential mediated flows. Devoid of any ad hoc simplifications, the framework which is constructed here to model such scenarios is, however, not amenable to analytical treatments. Hence, it requires the use of numerical techniques for its solution. For our purpose, we choose the finite element method as implemented in the COMSOL MULTIPHYSICS environment. Our numerical framework is first validated by way of comparison of the isothermal condition results, obtained from the same, with those from a well-established semianalytical formulation found in Ref. [48] (see Appendix); pertinently, Ref. [48] has formed the basis of a number of subsequent works dealing with streaming potential mediated flows [29,34–36,39,53,54,57,62]. The excellent agreement between the results, for the isothermal condition, obtained from the two methods sets a robust ground for using the present numerical framework in further investigations of the influence of the temperature gradient. In this regard, we show the importance of considering the Soret effect by comparing the results obtained by incorporating the temperature-gradient influences solely in the momentum equation, with those obtained by considering the influence of the temperature gradient on the ionic flux as well. Finally, we explicate the role of the Soret effect, and the consequential thermoelectric effect, in altering temperature-gradient mediated streaming potential flows, as embodied by the variations in the resulting flow rate, through its intrinsic influence on the ionic species transport. During this endeavor, we also highlight in a pinpointed manner the influence of electrothermal effects on such nonisothermal streaming potential flows by isolating its consequences from the other thermal effects. In this section, unless otherwise mentioned, we show all results corresponding to constant values of $\tilde{\zeta}_0 = -0.5$, $K = 10$, $C = 0.828$, $\alpha = 2.39 \times 10^{-6}$, and $\mathrm{Pe} = 6.85 \times 10^{-4}$. Also, as reference values of the ionic heat of transport of the cation, Q_+, and that of the anion, Q_-, typical values for an alkali halide are used [84]; corresponding values of $\mathcal{Q}$ and γ are 1.388 and 0.153 (in the ensuing discussion these values of $\mathcal{Q}$ and γ will be referred to as $\mathcal{Q}^*$ and γ^*). The dependence of viscosity, thermal conductivity, and permittivity on temperature is captured through the following

TABLE I. Values of the coefficients used to capture the temperature dependence of the viscosity, thermal conductivity, and the permittivity.

Coefficient	Value	Coefficient	Value
a_0	1.379957	b_0	-8.69×10^{-1}
a_1	-2.112402×10^{-2}	b_1	8.948×10^{-3}
a_2	1.360456×10^{-4}	b_2	-1.5836×10^{-5}
a_3	-4.64509×10^{-7}	b_3	7.9754×10^{-9}
a_4	8.904274×10^{-10}	c_0	251.1
a_5	$-9.079069 \times 10^{-13}$	c_1	-0.7992
a_6	3.845733×10^{-16}	c_2	7.375×10^{-4}

polynomial fit forms [104]:

$$\begin{aligned} \mu &= a_0 + a_1 T + a_2 T^2 + a_3 T^3 + a_4 T^4 + a_5 T^5 + a_6 T^6, \\ k &= b_0 + b_1 T + b_2 T^2 + b_3 T^3, \\ \epsilon &= 8.85 \times 10^{-12}(c_0 + c_1 T + c_2 T^2), \end{aligned}$$

where the values of the coefficients are given in Table I. Additionally, the diffusivity is known to increase by 2.5% for every degree rise in temperature [105], so that the form of the diffusivity dependence on temperature is taken to be

$$D_{\pm} = D_{\pm}^0\{1 + 0.025(T - T_0)\}.$$

The straightforward stratagem that one might expect to follow while investigating any thermal influence would be through the incorporation of such thermal gradients, emanating from osmotic pressure contributions (which otherwise remain latent in conventional isothermal treatments), in the momentum equation. While such an expectation is not wrong, it does not constitute the entire picture. For, even though the incorporation of temperature gradients in the momentum equation and the consequent influences on the velocity field may in turn be expected to influence the ionic flux leading to significantly coupled manifestation of such gradients in the overall field distributions, it still does not take into account the intrinsic dependence of the ionic species flux on the temperature gradient. Indeed, the influence of the temperature gradient on the ionic flux is deeply ingrained in the fundamental cross couplings associated with the nonequilibrium thermodynamics of general species transport; in particular, the Soret effect, as represented, within the present framework, by the term $\frac{D_{\pm} n_{\pm} Q_{\pm}}{k_B T^2}\nabla T$ in Eq. (2). It is this physical phenomenon that determines the transport of a particle in response to an applied temperature gradient.

As a first step in our discussion of the temperature-gradient influence on the overall transport problem, we show, through Fig. 2, the differences in the results obtained from the consideration of Soret effect as compared to the aforementioned intuitive (but physically incomplete) stratagem. Figure 2 shows the velocity profile across the cross section at $\tilde{x} = 0.5$. The plots with Soret effects incorporated are obtained for $\mathcal{Q} = \mathcal{Q}^*$ and $\gamma = 100\gamma^*$. The Soret effect is observed to suppress the magnitude of the velocity profile. This is particularly significant because it is the velocity profile which ultimately determines the volumetric flow rate and thus the throughput ratings of any micro- or nano-device. It is important to note that this suppression of the volumetric flow rate due to the

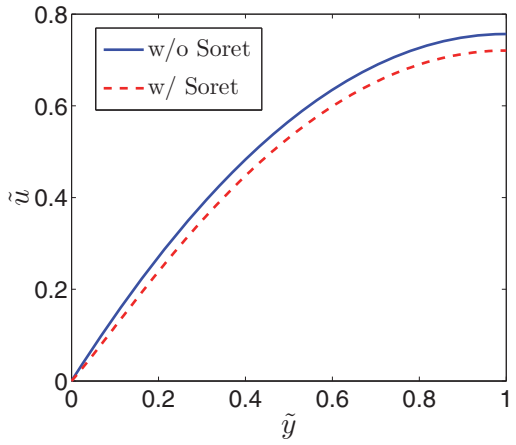

FIG. 2. (Color online) Comparison of the velocity profiles considering Soret effect and that without, along the cross section of the channel at $\tilde{x} = 0.5$ with $\tilde{\zeta}_0 = -0.5$, $K = 10$. Values of $\mathcal{Q} = \mathcal{Q}^*$ and $\gamma = 100\gamma^*$. Symbols "w" and "w/o" represent with and without the Soret effect, respectively. It is to be noted here that the thermal effects stemming from the osmotic pressure contributions in the momentum equation are considered in both the velocity profiles.

temperature-gradient influences is over and above that due to the streaming potential effects which invariably reduces the throughput in pressure-gradient-driven flows through the generation of a back potential that drives a self-induced back-electro-osmotic flow. A discussion of the reason behind the Soret effect induced suppression is in order.

Positive values of $\mathcal{Q}$ and γ, originating from positive values of Q_+ and Q_-, represent the thermophobic nature of the ions. This means that within the sole purview of the Soret effect (independent from any other electrokinetic or convective influences), these ions have a tendency to move from the hot to the cold region. Since temperature increases in the direction of the pressure-gradient-driven flow (as shown in Fig. 1), the thermodiffusive movement (associated purely with the Soret effect) of the ions is in the opposite direction. In perfect analogy with the physical explanation of the phenomenon of electro-osmosis, where it is the electrophoretic motion of the electrical double layer charges which gets translated into a motion of the fluid, so also in the current situation the back-thermodiffusive motion of the ions results, in turn, in a thermo-osmotic flow of the fluid. Since this temperature-gradient mediated backflow of the fluid is in the same direction as the streaming potential induced backflow, the applied temperature gradient is seen to further suppress the fluid flow compared to the case with no consideration of the Soret effect. It is important to note here that Fig. 2 simply justifies the importance of considering the influence of local temperature gradients on ionic transport for predicting the accurate flow rate for thermally mediated streaming potential flows by considering a particular value of $\mathcal{Q}$ and γ. However, in order to critically analyze the role of Soret effect, in its entirety, it is imperative to take into consideration the genesis and ramifications of the consequential thermoelectric effect, through a more exhaustive parametric study. This thermoelectric effect arises due to the accumulation of the ions which get transported in response to the Soret effect.

In order to obtain a clearer picture of the combined influences of the electrokinetic, Soret, and the as-yet unexplained thermoelectric effects, we investigate the extent to which the values of the Soret effect parameters $\mathcal{Q}$ and γ affect the volumetric flow rate. In both Figs. 3(a) and 3(b), we study the variation of the dimensionless volumetric flow rate over the half-channel cross section (defined to be $\int_0^1 \tilde{u} d\tilde{y}$) as the value of $\mathcal{Q}$ is varied around $\mathcal{Q}^*$ over four orders of magnitude, i.e., $-2 \leqslant \log_{10}(\mathcal{Q}/\mathcal{Q}^*) \leqslant 2$ for different values of γ. Here, we also make an attempt to isolate the role of the electrothermal effect in altering the flow characteristics. To this end, in Fig. 3(a) we consider the electrothermal effects based on the temperature dependence of the permittivity, whereas in Fig. 3(b) we do not consider the electrothermal effects. While both Figs. 3(a) and 3(b) show qualitatively similar trends, there are significant quantitative differences between them as clearly shown in Fig. 3(c). In what follows, we first justify these similar qualitative trends, and then discuss the reasons for the quantitative differences by taking into consideration the electrothermal effect.

For the explanation of the qualitative trends, we first observe that based solely on the explanation of the temperature-gradient-driven backflow of the ions (with the concomitant backflow of the fluid), presented in relation to Fig. 2, it would be natural to expect that the volumetric flow rate would decrease with increase in the value of $\mathcal{Q}$. However, in reality we observe that the value of the volumetric flow rate Q is practically constant until about $\log_{10} \mathcal{Q}/\mathcal{Q}^* \sim 0.5$, beyond which it rapidly increases or decreases depending on the magnitude of γ. The increase in the volumetric flow rate clearly proves that the explanation based on the simple backflow of the fluid, due to the back-thermodiffusive motion of the ions, does not capture the complete physical picture of the Soret effect, and is strongly indicative of the presence of more involved phenomena. To understand this, it is to be first noted that the unequal values of the ionic heat of transport of the counterions (in our case the cations) and the coions (in our case the anions) determine the extent of their thermophobicity, and hence dictate the strength of their motion away from the hotter region. Therefore, the lower value of the ionic heat of transport of the coions (anions) than that of the counterions (cations), as represented by $\gamma < 1$ (i.e., $\gamma < 10\gamma^*$), ensures that the counterions have a greater propensity of migrating upstream, i.e., towards the region of lower temperature, than the coions. Additionally, since the number density of the counterions is higher than that of the coions, there is a predominant accumulation of the counterions in the upstream region; this segregation of the ions then leads to the generation of a thermoelectric field where the potential drops down along the direction opposite to that of the temperature-gradient induced motion of the ions. In our case, this is also the direction of the primary pressure-gradient-driven flow. Hence, for $\gamma < 10\gamma^*$, the thermoelectric field opposes the streaming potential field. Consequently, it also opposes the further flow of counterions in the upstream direction in response to both the temperature-gradient induced thermodiffusion and the streaming potential mediated back-electro-osmosis. This ultimately leads to a decrease in the suppression of the pressure-gradient-driven volumetric flow rate. Now, at a particular value of γ, satisfying the condition

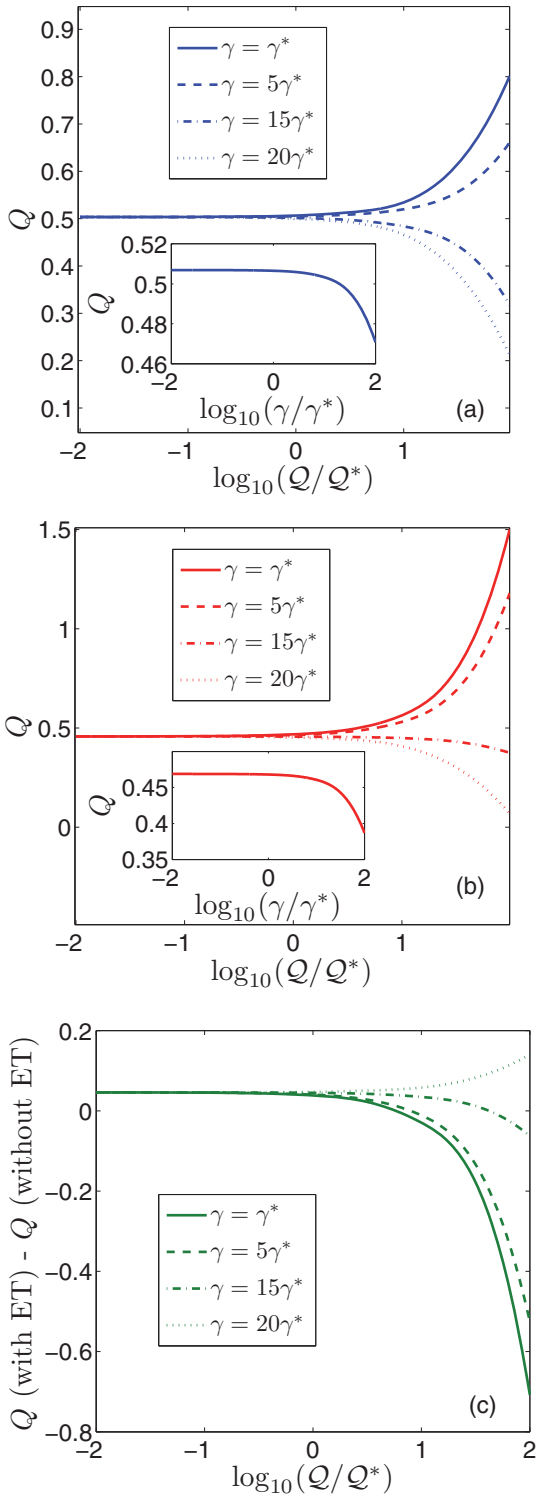

FIG. 3. (Color online) Variation of the dimensionless volumetric flow rate corresponding to the variation of $\mathcal{Q}/\mathcal{Q}^*$ over four orders of magnitude for four different values of γ/γ^*. In (a) electrothermal effects are considered, and in (b) electrothermal effects are not considered; inset shows the variation of the dimensionless volumetric flow rate with γ/γ^* varying over four orders of magnitude. In (c) differences in the volumetric flow rates with and without considering electrothermal effects are shown. The values of $\tilde{\zeta}_0 = -0.5$, $K = 10$, and $T_{\text{ratio}} = 1.17$ are kept constant.

$\gamma < 10\gamma^*$, with increasing value of $\mathcal{Q}$, the strength of the thermoelectric field increases. Therefore, the suppression of the primary flow continually decreases, and consequently, the volumetric throughput progressively increases.

As the value of γ increases towards 1, i.e., as the difference in the values of the ionic heat of transport of the counterions and the coions decreases, there is smaller manifestation of the thermoelectric effect. This can be clearly perceived in Fig. 3 where the volumetric flow rate decreases for $\gamma = 5\gamma^*$, as compared to $\gamma = \gamma^*$, implying that the thermoelectric field is now relatively weaker so that it cannot counteract the volumetric flow resistance, due to streaming potential induced backflow and the thermodiffusive motion of ions, to a greater extent. For the value $\gamma = 1$ (this is true for $\gamma \sim 10\gamma^*$), the thermoelectric field will be solely determined by the predominance in the number density of the counterions. Further increase in the value of γ beyond 1, i.e., $\gamma > 10\gamma^*$, leads to a reversal in the nature of the thermoelectric field. Indeed, with γ now being greater than 1 (implying $\mathcal{Q}_- > \mathcal{Q}_+$), it is the coions (anions for our case) which have a greater propensity to flow upstream compared to the counterions: This leads to an inversion in the polarity of the thermoelectric field. Consequently, this thermoelectric field is now directed opposite to the pressure-gradient-driven flow, and aids the streaming potential mediated back-electro-osmotic flow leading to a significant decrease in the overall volumetric flow as seen in Fig. 3 for the plots corresponding to $\gamma = 15\gamma^*$ and $\gamma = 20\gamma^*$. Moreover, as mentioned before, the stronger the thermophobicity of the ions indicated by higher (positive) values of the ionic heats of transport, the stronger is the Soret effect induced backmigration of ions and the higher is the magnitude of the thermoelectric field: This explains the strong decrement in the values of the overall volumetric flow rate for higher values of $\log_{10}\mathcal{Q}/\mathcal{Q}^*$, for $\gamma > 10\gamma^*$. As a further validation of the aforementioned explanation, the inset of Fig. 4 clearly shows the decreasing trend in the volumetric flow rate with increasing value of γ relative to γ^* for a constant value of $\mathcal{Q} = \mathcal{Q}^*$. An important point to remember is that irrespective of the values of $\mathcal{Q}$ and γ, the combined consequences of the thermoelectric field, the Soret effect, and the streaming potential mediated flows are fundamentally determined by the criterion that the net ionic current across any cross section of the channel should necessarily be zero in the stationary state.

The quantitative differences between Figs. 3(a) and 3(b), as graphically represented in Fig. 3(c), arise due to the consideration of the electrothermal effect stemming from the temperature-dependent permittivity variation [electrothermal effects are present in the case of Fig. 3(a) and absent in the case of Fig. 3(b)]. We note that a reference Debye length, λ_0, has been defined earlier based on the permittivity at T_0. However, if the permittivity is temperature dependent, then the local Debye screening length, λ, along the wall will be a function of the temperature (and will thus be different from λ_0). As the temperature increases, the permittivity, ϵ, decreases. Since $\lambda \sim \epsilon^{1/2}$, the Debye screening length decreases along the wall, too. This means that as the temperature increases along the wall, the local penetration of the diffuse layer of the EDL into the bulk decreases. This is of immediate consequence to the streaming potential. A reduced penetration of the diffuse layer means that there will be a reduced streaming current

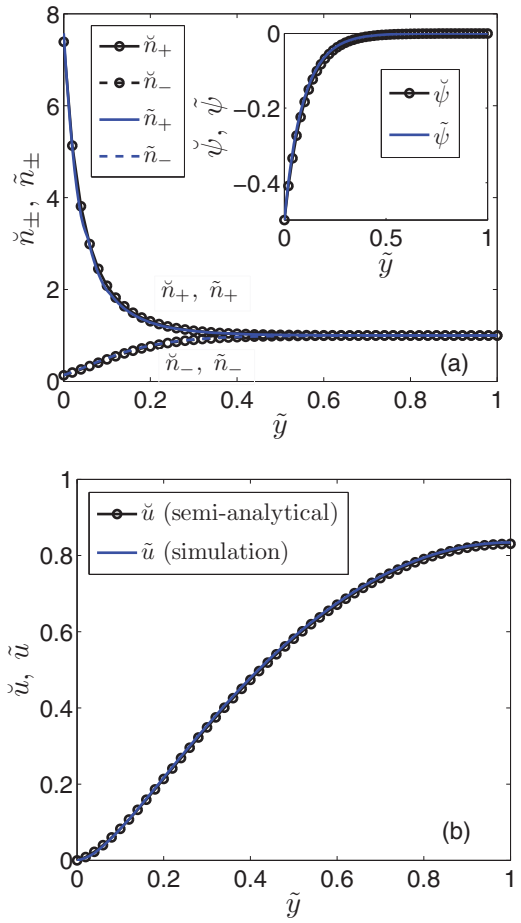

FIG. 4. (Color online) (a) Number density of counterions and coions along the cross -section at $\tilde{x} = 0.5$ corresponding to $\breve{\zeta} = -0.5$ and $K = 10$ and in the absence of any temperature gradient. Inset shows the corresponding electrokinetic screening potential profile. (b) The corresponding axial direction velocity profile. The plots with markers represent the results from the semianalytical formulation [48] while those without represent the results from the numerical framework developed in this study. These results are found to be in excellent agreement.

(as a larger portion of the electroneutral region will now be in the path of the pressure-gradient-driven flow) which will lead to a lower streaming potential. This, in turn, will lead to a lower streaming potential induced backflow, ultimately resulting in a reduced volumetric suppression. Hence, the pressure-gradient-driven volumetric throughput is more for the case considering electrothermal effect than that obtained without it. This culminates in an almost constant positive value of the difference in volumetric flow rates with and without considering electrothermal effects, as plotted in Fig. 3(c). This physical picture is true only up to $\log_{10} \mathcal{Q}/\mathcal{Q}^* \sim 0.5$, a regime where the streaming potential effects predominate. Beyond this, as discussed previously, the thermoelectric effects supersede the streaming potential effects (either opposing it or aiding it depending on the value of γ). However, in this regime too, the reduced penetration of the diffuse layer of the EDL, on considering the electrothermal effect, results in a reduced thermoelectric field. This is so because a greater part of the channel region is now covered by the electroneutral zone (with equal number densities of the counterions and coions). Therefore, for lower values of γ ($\gamma < 1$, which holds true for $\gamma < 10\gamma^*$; this implies that the ionic heat of transport of the counterion is higher), when the thermoelectric field is directed opposite to the direction of the streaming potential field, the volumetric flow rate does increase compared to the $\log_{10} \mathcal{Q}/\mathcal{Q}^* < 0.5$, but it is significantly less than the case when no electrothermal effects are considered due to the weaker thermoelectric effect. This manifests in increasingly negative values of the difference in volumetric flow rates with and without considering electrothermal effects, for lower values of γ, as can be seen in Fig. 3(c).

For higher values of γ ($\gamma > 1$, which holds for $\gamma > 10\gamma^*$), it is the coions which have a greater propensity for backflow compared to the counterions due to the Soret effect, and this results in a thermoelectric field having the same direction as the streaming potential field. However, the electrothermal effects with the resultant reduced penetration of the diffuse layer gives rise to a reduced thermoelectric field. This weakened thermoelectric field does reinforce the volumetric suppression due to the streaming potential field, but this reinforcement is less than in the case without considering electrothermal effects. Hence, the resulting flow rate is more for the case with electrothermal effect, than that obtained without it. This trend is also clearly observed in Fig. 3(c), where the difference between the volumetric flow rates obtained with and without considering electrothermal effects becomes positive for higher values of γ.

Finally, to put the aforementioned observations in a realistic perspective, we mention here the real values of volumetric throughputs for thermally mediated streaming potential flows, as obtained from the present theoretical framework for certain practically realizable situations. The numerical values of the flow rates presented here correspond to $u_{\text{ref}} = 2.86$ μm/s. Let us first consider the case with the electrothermal effect which addresses the most general scenario. Now, for $Q_+ = 5.744 \times 10^{-22}$ J, which conforms to the streaming potential dominated flow regime (i.e., $\log_{10} \mathcal{Q}/\mathcal{Q}^* \leqslant 0.5$), the actual volumetric flow rate is obtained to be $Q_{\text{dim}} = 34.4$ pl (picoliter). Accordingly, for a greater value of the ionic heat of transport of the cation $Q_+ = 5.744 \times 10^{-19}$ J, which satisfies the condition $\log_{10} \mathcal{Q}/\mathcal{Q}^* > 0.5$, the volumetric flow rate is found to be $Q_{\text{dim}} = 54.35$ pl (i.e., 57.99% increase compared to the flow rate in the streaming potential dominated regime) for $\gamma = \gamma^*$, and $Q_{\text{dim}} = 13.9$ pL (i.e., 59.59% decrease compared to the flow rate in the streaming potential dominated regime) for $\gamma = 20\gamma^*$ (values of all the other parameters being identical). This unambiguously proves that the role of the Soret effect, and the consequential thermoelectric effect, in opposing or aiding the streaming potential field induced suppression of the volumetric flow rate is quite significant, and hence, cannot be trivially precluded from any theoretical analysis pertaining to nonisothermal streaming potential flows. Now, on neglecting the electrothermal effect, the volumetric flow rate is obtained to be $Q_{\text{dim}} = 103.83$ pl for $\gamma = \gamma^*$, and $Q_{\text{dim}} = 4.33$ pl for $\gamma = 20\gamma^*$, corresponding to the same value of the ionic heat of transport ($Q_+ = 5.744 \times 10^{-19}$ J). This validates the observation that the electrothermal effect weakens the thermoelectric field. So, when electrothermal effects are not considered, it results in a stronger suppression of the flow rate (compared to the case where electrothermal effects are

considered) for the cases where the thermoelectric field and the streaming potential field are directed opposite to each other. However, where the two fields reinforce each other in inducing a backflow, there is a reduced flow rate suppression (compared again to the case where electrothermal effects are considered).

V. SUMMARY AND CONCLUSIONS

In this study, we clearly delineate the as-yet unaddressed temperature-gradient induced alterations of the streaming potential mediated pressure-gradient-driven flows. These alterations primarily stem from the intrinsic dependence of the ionic flux on the local temperature gradients, as coherently captured in our modeling framework by the inclusion of the Soret effect. In this regard, we clearly show that the inclusion of the Soret effect significantly alters the velocity profiles, and hence its consideration is imperative for accurate prediction of the electrohydrodynamic characteristics pertaining to nonisothermal streaming potential flows. We unambiguously prove that the resulting volumetric flow rate of such nonisothermal streaming potential flows stems from the combined interplay of electrokinetic effects, Soret effect, and the consequential thermoelectric effect, which arises due to the differences in the ionic heats of transport of the cations and the anions. This realization paves the way for the most important finding of our study: We show here, that depending on the polarity of the generated thermoelectric field, which is determined by the relative thermodiffusive migration strengths of the cations and the anions, the suppression of the volumetric flow rate due to the streaming potential field may be opposed or aided. Hence, the simple imposition of an external temperature gradient provides an additional control over the volumetric flow rate for streaming potential flows through the Soret effect and the concomitant thermoelectric field. This control over the resulting flow rate can be exercised, for a definite magnitude of the externally applied temperature gradient, by simply changing the nature of the electrolyte. Finally, we also highlight, in a pinpointed manner, the role of the electrothermal effect in the observed alterations of the temperature-gradient mediated streaming potential flows. The electrothermal effect basically weakens the thermoelectric field leading to reduced flow rate, as compared to the case without electrothermal effects, when the thermoelectric and streaming potential fields are opposing each other, and enhanced flow rate, when the thermoelectric field and the streaming potential field are oriented along the same direction. So, based on the findings of our work, it can be definitely concluded that temperature gradients can be successfully employed for tuning streaming potential mediated flows. Moreover, the implications of this endeavor hold the promise of addressing a new paradigm of microfluidic devices that relies on strong thermoelectrical coupling.

The influence of the Soret effect and the consequential thermoelectric effect on the flow characteristics of nonisothermal streaming potential flows, as delineated here, can be experimentally verified (or practically realized) by measuring the flow rates at the outlet reservoir, for normal pressure-driven flows of electrolyte solutions through polydimethylsiloxane (PDMS)-glass microchannels. To this end, the temperature gradient on the channel walls can be imposed by maintaining hot water and cold water reservoirs at the two ends of the channel. However, for implementing a linear temperature gradient at the channel walls, as done in the present work, it is sufficient to maintain a constant heat flux at the walls [106]. For a definite magnitude of the wall temperature gradient, flows of different electrolytes (having different magnitudes of the ionic heats of transport) can be sustained through the microchannel by means of a syringe pump, and the resulting flow rate at the outlet can be simultaneously measured by a suitable flowmeter. A comparison of the outlet flow rates, for different electrolytes, will clearly highlight the influence of the thermal effects on streaming potential mediated flows. However, such an extensive experimental endeavor is beyond the scope of the present work, and can be the premise of a separate research work.

ACKNOWLEDGMENTS

J.C. thanks Dr. Mathias Dietzel at the Centre of Smart Interfaces (CSI), Technische Universität Darmstadt for an important discussion related to the osmotic pressure. J.C. and S.C. thank Prof. Steffen Hardt for hosting them at the CSI while the initial version of this manuscript was under preparation.

APPENDIX: VALIDATION OF SIMULATION RESULTS

For the sake of this validation study, we first switch off the influence of the temperature gradient in our numerical framework by setting $T_{\text{ratio}} = 1$. Next, we restate the dimensionless axial direction velocity from the semianalytical formulation of Ref. [48] in a suitably modified nondimensional format to make the representation amenable for meaningful comparisons with the present formulation. The axial velocity, in accordance with Ref. [48], can be expressed as

$$\breve{u} = (2\tilde{y} - \tilde{y}^2) - 8\frac{C\breve{E}_s}{K^2}\tilde{\zeta}\left(1 - \frac{\tilde{\psi}}{\tilde{\zeta}}\right). \tag{A1}$$

Here the dimensionless streaming potential ($\breve{E}_s$) is given by

$$\breve{E}_s = \frac{\frac{1}{\alpha}\text{Pe}I_{1s}}{I_{2s} - 8\frac{C\text{Pe}}{\alpha K^2}I_{3s}}, \tag{A2}$$

where the expressions of the three integrals are

$$I_{1s} = \int_0^2 (\breve{n}_+ - \breve{n}_-)(\tilde{y}^2 - 2\tilde{y})\, d\tilde{y}, \tag{A3}$$

$$I_{2s} = \int_0^2 (\breve{n}_+ + \breve{n}_-)\, d\tilde{y}, \tag{A4}$$

$$I_{3s} = \int_0^2 \breve{\zeta}(\breve{n}_+ - \breve{n}_-)\left(1 - \frac{\breve{\psi}}{\breve{\zeta}}\right) d\tilde{y}. \tag{A5}$$

It is to be noted that in this formulation, the electrokinetic potential profile is obtained by solving the Poisson equation:

$$\frac{\partial^2\breve{\psi}}{\partial\tilde{y}^2} = -\frac{1}{8}K^2(\breve{n}_+ - \breve{n}_-), \tag{A6}$$

where the ionic number densities are assumed to follow the Boltzmann distribution: $\breve{n}_\pm = \exp(\mp 4\breve{\psi})$.

In Fig. 4(a), we show the distribution of the number density of the counterions and the coions along the cross section of the channel at $\tilde{x} = 0.5$ obtained from both the

numerical implementation and the semianalytical formulation. We also show, in the inset of Fig. 4(a), the comparison of the electrokinetic potential profile, accompanying the ion distribution, obtained from the two methods. Furthermore, in Fig. 4(b), we show the corresponding velocity profiles obtained from the two methods. All the results from the two methods are found to be in excellent agreement, thereby establishing the accuracy of the present numerical framework.

[1] R. J. Hunter, *Foundations of Colloid Science*, 2nd ed. (Oxford University Press, New York, 2001).
[2] G. Quincke, Ann. Phys. **189**, 513 (1861).
[3] S. P. Fritton and S. Weinbaum, Annu. Rev. Fluid Mech. **41**, 347 (2009).
[4] R. C. Riddle and H. J. Donahue, J. Orthop. Res. **27**, 143 (2009).
[5] L. Han, A. J. Grodzinsky, and C. Ortiz, Annu. Rev. Mater. Res. **41**, 133 (2011).
[6] R. Snieder, S. Hubbard, M. Haney, G. Bawden, P. Hatchell, A. Revil, and DOE Geophysical Monitoring Working Group, Annu. Rev. Earth Planet Sci. **35**, 653 (2007).
[7] R. A. van Wagenen and J. D. Andrade, J. Colloid Interface Sci. **76**, 305 (1980).
[8] C. Werner, H. Körber, R. Zimmermann, S. Dukhin, and H.-J. Jacobasch, J. Colloid Interface Sci. **208**, 329 (1998).
[9] D. Erickson and D. Li, J. Colloid Interface Sci. **237**, 283 (2001).
[10] Y. Min, N. Pesika, J. Zasadzinski, and J. Israelachvili, Langmuir **26**, 8684 (2010).
[11] A. M. Gallardo-Moreno, V. Vadillo-Rodriguez, J. Perera-Nunez, J. M. Bruque, and M. L. Gonzalez-Martin, Phys. Chem. Chem. Phys. **14**, 9758 (2012).
[12] J. F. Osterle, J. Appl. Mech. **31**, 161 (1964).
[13] F. A. Morrison and J. F. Osterle, J. Chem. Phys. **43**, 2111 (1965).
[14] R. C. Srivastava and A. K. Jain, J. Hydrol. **25**, 339 (1975).
[15] J. Yang, F. Lu, L. W. Kostiuk, and D. Y. Kwok, J. Micromech. Microeng. **13**, 963 (2003).
[16] H. Daiguji, P. Yang, A. J. Szeri, and A. Majumdar, Nano Lett. **4**, 2315 (2004).
[17] W. Olthius, B. Schippers, J. Eijkel, and A. van den Berg, Sens. Actuators, B **111-112**, 385 (2005).
[18] J. Yang, F. Lu, L. W. Kostiuk, and D. Y. Kwok, J. Nanosci. Nanotechnol. **5**, 648 (2005).
[19] F. H. J. van der Heyden, D. J. Bonthius, D. Stein, C. Meyer, and C. Dekker, Nano Lett. **6**, 2232 (2006).
[20] M.-C. Lu, S. Satyanarayana, R. Karnik, A. Majumdar, and C.-C. Wang, J. Micromech. Microeng. **16**, 667 (2006).
[21] F. H. J. van der Heyden, D. J. Bonthius, D. Stein, C. Meyer, and C. Dekker, Nano Lett. **7**, 1022 (2007).
[22] S. Pennathur, J. C. T. Eijkel, and A. van den Berg, Lab Chip **7**, 1234 (2007).
[23] C. Davidson and X. Xuan, J. Power Sources **179**, 297 (2008).
[24] C. Davidson and X. Xuan, Electrophoresis **29**, 1125 (2008).
[25] Y. Ren and D. Stein, Nanotechnology **19**, 195707 (2008).
[26] Y. Xie, X. Wang, J. Xue, K. Jin, and L. C. Y. Wang, Appl. Phys. Lett. **93**, 163116 (2008).
[27] A. M. Duffin and R. J. Saykally, J. Phys. Chem. C **112**, 17018 (2008).
[28] R. Chein, C. Liao, and H. Chen, J. Power Sources **187**, 461 (2009).
[29] F. Munshi and S. Chakraborty, Phys. Fluids **21**, 122003 (2009).
[30] M. Wang and Q. Kang, Microfluid. Nanofluid. **9**, 181 (2010).
[31] C.-C. Chang and R.-J. Yang, Microfluid. Nanofluid. **9**, 225 (2010).
[32] C. L. A. Berli, J. Colloid Interface Sci. **349**, 446 (2010).
[33] R. Chein, K. Tsai, and L. Yeh, Electrophoresis **31**, 535 (2010).
[34] P. Goswami and S. Chakraborty, Langmuir **26**, 581 (2010).
[35] A. Garai and S. Chakraborty, Electrophoresis **31**, 843 (2010).
[36] A. Bandopadhyay and S. Chakraborty, Langmuir **27**, 12243 (2011); Appl. Phys. Lett. **101**, 043905 (2012).
[37] D. Gillespie, Nano Lett. **12**, 1410 (2012).
[38] A. Mansouri, S. Bhattacharjee, and L. Kostiuk, Lab Chip **12**, 4033 (2012).
[39] A. Bandopadhyay, J. Dhar, and S. Chakraborty, Phys. Rev. E **88**, 033014 (2013).
[40] G. A. H. Elton, Proc. R. Soc. London, Ser. A **194**, 259 (1948).
[41] G. A. H. Elton and F. G. Hirschler, Proc. R. Soc. London, Ser. A **198**, 581 (1949).
[42] D. Burgreen and F. R. Nakache, J. Phys. Chem. **68**, 1084 (1964).
[43] C. L. Rice and R. Whitehead, J. Phys. Chem. **69**, 4017 (1965).
[44] S. Levine, J. R. Marriott, G. Neale, and N. Epstein, J. Colloid Interface Sci. **52**, 136 (1975).
[45] E. Donath and A. Voigt, J. Colloid Interface Sci. **109**, 122 (1986).
[46] J. D. Sherwood, Phys. Fluids **19**, 053101 (2007).
[47] J. D. Sherwood, Langmuir **24**, 10011 (2008).
[48] S. Chakraborty and S. Das, Phys. Rev. E **77**, 037303 (2008).
[49] X. Xuan, Microfluid. Nanofluid. **4**, 457 (2008).
[50] J. D. Sherwood, Phys. Fluids **21**, 013101 (2009).
[51] E. Lac and J. D. Sherwood, J. Fluid Mech. **640**, 55 (2009).
[52] H. M. Park and J. Y. Lim, J. Colloid Interface Sci. **336**, 834 (2009).
[53] S. Das and S. Chakraborty, Langmuir **25**, 9863 (2009).
[54] T. Das, S. Das, and S. Chakraborty, J. Chem. Phys. **130**, 244904 (2009).
[55] M. Wang, C.-C. Chang, and R.-J. Yang, J. Chem. Phys. **132**, 024701 (2010).
[56] S. Das and S. Chakraborty, Langmuir **26**, 11589 (2010).
[57] J. Chakraborty and S. Chakraborty, Phys. Fluids **22**, 122002 (2010); **23**, 082004 (2011).
[58] E. Yariv, O. Schnitzer, and I. Frankel, J. Fluid Mech. **685**, 306 (2011); O. Schnitzer, I. Frankel, and E. Yariv, *ibid.* **704**, 109 (2012).
[59] O. Schnitzer, A. S. Khair, and E. Yariv, Phys. Rev. Lett. **107**, 278301 (2011);
[60] H. Zhao, Phys. Fluids **23**, 022003 (2011).
[61] I. Dumitrescu, R. K. Anand, S. E. Fosdick, and R. M. Crooks, J. Am. Chem. Soc. **133**, 4687 (2011).
[62] J. Chakraborty, S. Ray, and S. Chakraborty, Electrophoresis **33**, 419 (2012); A. Shenoy, J. Chakraborty, and S. Chakraborty, *ibid.* **34**, 691 (2013); J. Dhar, U. Ghosh, and S. Chakraborty, *ibid.*, doi: 10.1002/elps.201300428.

[63] J. Chakraborty, R. Dey, and S. Chakraborty, Phys. Rev. E. **86**, 061504 (2012); A. Bandopadhyay and S. Chakraborty, Langmuir **28**, 17552 (2012).
[64] U. Ghosh and S. Chakraborty, Phys. Rev. E **88**, 033001 (2013).
[65] J. Chakraborty and S. Chakraborty, Phys. Rev. E **88**, 043007 (2013).
[66] G. M. Mala, D. Li, and J. D. Dale, Int. J. Heat Mass Transfer **40**, 3079 (1997).
[67] D. Maynes and B. W. Webb, J. Heat Transfer **125**, 889 (2003).
[68] S. Chakraborty, Int. J. Heat Mass Transfer **49**, 810 (2006).
[69] S. T. Tan and E. Y. K. Ng, Numer. Heat Transfer, Part A **49**, 991 (2006).
[70] A. Elazhary and H. M. Soliman, Int. J. Heat Mass Transfer **52**, 4449 (2009).
[71] A. Sadeghi and M. H. Saidi, Int. J. Heat Mass Transfer **53**, 3782 (2010).
[72] P. W. Hwang and C. Y. Soong, Int. J. Heat Mass Transfer **51**, 210 (2008).
[73] H. S. Kwak, H. Kim, J. M. Hyun, and T.-H. Song, J. Colloid Interface Sci. **335**, 123 (2009).
[74] H. Yavari, A. Sadeghi, H. M. Saidi, and S. Chakraborty, Int. J. Heat Mass Transfer **55**, 762 (2012).
[75] S. R. de Groot and P. Mazur, *Non-equilibrium Thermodynamics* (North Holland, Amsterdam, 1962).
[76] D. Kondepudi and I. Prigogine, *Modern Thermodynamics: From Heat Engines to Dissipative Structures* (John Wiley, New York, 1998).
[77] B. Baranowski, J. Membr. Sci. **57**, 119 (1991).
[78] J. Newman and K. E. Thomas-Alyea, *Electrochemical Systems*, 3rd ed. (Wiley-Interscience, Hoboken, NJ, 2004).
[79] G. R. Engelhardt, S. N. Lvov, and D. D. Macdonald, J. Electroanal. Chem. **429**, 193 (1997).
[80] B. V. Derjaguin, N. V. Churaev, and V. M. Muller, *Surface Forces* (Plenum, New York, 1987).
[81] J. L. Anderson, Annu. Rev. Fluid Mech. **21**, 61 (1989).
[82] M. Dietzel and S. Hardt, *Proceedings of the 3rd European Conference on Microfluidics* (Microfluidics, Heidelberg, 2012).
[83] S. A. Putnam and D. G. Cahill, Langmuir **21**, 5317 (2005).
[84] A. Würger, Phys. Rev. Lett. **101**, 108302 (2008).
[85] S. N. Rasuli and R. Golestanian, Phys. Rev. Lett. **101**, 108301 (2008).
[86] J. Morthomas and A. Würger, Eur. Phys. J. E **27**, 425 (2008).
[87] S. Fayolle, T. Bickel, and A. Würger, Phys. Rev. E **77**, 041404 (2008).
[88] A. Würger, Langmuir **25**, 6696 (2009).
[89] J. Morthomas and A. Würger, J. Phys.: Condens. Matter **21**, 035103 (2009).
[90] A. Würger, Rep. Prog. Phys. **73**, 126601 (2010).
[91] D. Vigolo, S. Buzzaccaro, and R. Piazza, Langmuir **26**, 7792 (2010).
[92] M. Bonetti, S. Nakamae, M. Roger, and P. Guenoun, J. Chem. Phys. **134**, 114513 (2011).
[93] A. Majee and A. Würger, Phys. Rev. Lett. **108**, 118301 (2012).
[94] G. Guthrie, J. N. Wilson, and V. Schomaker, J. Chem. Phys. **17**, 310 (1949).
[95] E. Ruckenstein, J. Colloid Interface Sci. **83**, 77 (1981).
[96] K. I. Morozov, JETP **88**, 944 (1999).
[97] D. Vigolo, R. Rusconi, H. A. Stone, and R. Piazza, Soft Matter **6**, 3489 (2010).
[98] C. Ludwig, Sitzungsber. Akad. Wiss. Wien, Math.-Naturwiss. Kl. **20**, 539 (1859).
[99] C. Soret, Arch. Sci. Phys. Nat. **2**, 48 (1879).
[100] R. F. Probstein, *Physicochemical Hydrodynamics*, 2nd ed. (Wiley-Interscience, Hoboken, NJ, 2003).
[101] T. Ishido and H. Mizutani, J. Geophys. Res. **86**, 1763 (1981).
[102] A. Revil, P. A. Pezard, and P. W. J. Glover, J. Geophys. Res. **104**, 20021 (1999).
[103] P. M. Reppert and F. D. Morgan, J. Geophys. Res. **108**, 2546 (2003).
[104] B. G. Hawkins and B. J. Kirby, Electrophoresis **31**, 3622 (2010).
[105] in *CRC Handbook of Chemistry and Physics*, edited by D. R. Lide (CRC Press, Boca Raton, FL, 2005).
[106] F. P. Incropera and D. P. DeWitt, *Fundamentals of Heat and Mass Transfer*, 5th ed. (John Wiley & Sons, Singapore, 2005).